

In situ strengthening of titanium with yttrium

A. M. RUSSELL, T. W. ELLIS, L. S. CHUMBLEY
Ames Laboratory, Iowa State University, Ames, IA 50011, USA

In situ processing consists of heavily deforming a two-phase alloy of mutually immiscible elements to produce composite sheet or wire. In the well-studied Cu(fcc)–Nb(bcc) system, severe deformation by swaging and drawing reduces niobium filament phase thicknesses from 1–5 μm (as-cast) to 0.007–0.030 μm (after deformation). Cu–20% (vol.) Nb ultimate tensile strengths exceed 2000 MPa for material deformed to a true strain of $\eta = 12$, where $\eta = \ln(\text{area}_{\text{original}}/\text{area}_{\text{final}})$. In a study on *in situ* strengthening in immiscible hexagonal close-packed metals, Ti–50 wt % Y and Ti–20 wt % Y alloys were deformed by hot extrusion, hot swaging, and cold swaging. As deformation progressed, samples were taken for tensile testing and examination by SEM and TEM. Ti–Y alloys deformed to final true strains of 6.6 (Ti–50Y) and 7.6 (Ti–20Y) contain nanofilaments (100 nm phase spacing) similar to those of deformation-processed Cu–20Nb at comparable strains. The ultimate tensile strengths of the alloys approximately tripled as deformation progressed from the as-cast condition to these final true strains, although the exponential strength increase seen in Cu–Nb alloys was not observed.

1. Introduction

1.1. *In situ* composite Cu–X alloys

During the last few years, a new class of copper–refractory metal alloys (Cu–X) has been developed with extraordinary mechanical and electrical properties [1–3]. These alloys, comprised of copper (fcc) with 10%–30% element X (where X is a bcc metal immiscible in copper such as niobium, vanadium, tantalum, chromium or iron), are severely deformed to produce a nanometre-scale microstructure of X filaments (when deformed by drawing) or lamellae (by rolling) in the copper matrix. The Cu–20%Nb system is the most thoroughly studied of these alloys and has ultimate tensile strengths exceeding 2000 MPa after deformation to a true strain of $\eta = 12$ (where $\eta = \ln[\text{initial cross-sectional area}/\text{final cross-sectional area}]$) [4].

The Cu–X alloys are characterized by remarkable ductility, which allows cast or powder-processed starting billets to be deformed to as much as $\eta = 13.4$ before breaking [5]. Such deformations represent more than an 800-fold reduction in diameter and are accompanied by a concomitant reduction in the thickness and spacing of the X phase. Thus, an as-cast billet of Cu–20Nb, displaying niobium dendrites of average thickness 5 μm and average spacing 25 μm , may be deformation-processed at room temperature into a wire with niobium filaments averaging 7 nm thick and 12 nm apart [6]. Such *in situ* processed composite alloys have strengths substantially higher than those of any other copper alloy. Debate continues on the mechanism(s) which account for the very high strengths of the Cu–X alloys [7–11], but discussion centres around the role of the nanofilamentary X structure in impeding propagation and motion of dislocations in both the copper and X phases.

1.2. *In situ* composite titanium alloys

In an attempt to produce an hcp *in situ* composite alloy, candidate metals were sought possessing good ductility, a phase diagram with mutual immiscibility and without intermetallic compounds, and roughly similar mechanical properties and melting temperatures. One combination of hcp metals meeting these criteria is a Ti–Y alloy. It was hoped that investigation of the deformation processing behaviour of such an hcp–hcp alloy might provide insights into the fundamental mechanism(s) operating in *in situ* composite alloys. In addition, if deformation processing proved to be a successful strengthening method in this system, a potentially useful low-density high-strength alloy might result.

2. Experimental procedures

2.1. Alloy preparation and deformation

2.1.1. Ti–50Y

High-purity titanium and yttrium (99.9%) were arc-melted into fingers of Ti–50 wt% Y and consumably drop cast into a chilled copper mould. The resulting 31 mm diameter ingot was jacketed in an evacuated steel can and extruded at 860 °C to $\eta = 2.8$. One portion (Path I) of the extruded material was further deformed by swaging at 725 °C, from $\eta = 2.8$ –4.8. The specimens could not be hot worked to strains greater than $\eta = 4.8$, because specimens of this size are too fine to retain their furnace heat during hot swaging. The protective steel jackets must also be removed at this size (about 2.5 mm), because they are difficult to machine away at smaller diameters. Beyond $\eta = 4.8$, deformation continued by swaging at room temperature with periodic stress-relief anneals in vacuum at 615 °C for 20 min after each 20% reduction in area.

These anneals are necessary to avoid cracking because unlike copper, titanium does not undergo dynamic recovery and recrystallization at room temperature. Cold swaging in this manner continued to a final diameter of 1.1 mm ($\eta = 6.6$) at which point the samples began to suffer from end cracking and surface exfoliation.

A second portion (Path II) of the hot-extruded Ti-50Y ingot was swaged at room temperature with the same periodic vacuum annealing from $\eta = 2.8$ –6.4 in an unsuccessful attempt to achieve a higher η value. The inability of the Ti-50Y alloy to tolerate higher levels of deformation is probably at least partially attributable to the inadvertent oxygen contamination of this alloy described more fully in Section 3.2.

2.1.2. Ti-20Y

A Ti-20 wt % Y specimen was prepared from high-purity (99.9%) titanium and yttrium as an arc-melted finger, 17 mm diameter, and jacketed in an argon-filled steel can. This specimen was swaged at 630 °C from $\eta = 0$ –2.0, followed by room-temperature swaging with the same vacuum annealing for stress relief used with the Ti-50Y samples. The steel jacket was removed when the specimen diameter reached 2.5 mm ($\eta = 3.8$), and room-temperature swaging continued to a final diameter of 0.4 mm ($\eta = 7.6$). At this final diameter, the specimen showed no cracking, but further deformation was not attempted because the specimen diameter was too fine for reliable tensile testing.

2.2. Tensile testing procedures and ductility measurements

All tensile test specimens larger than 1.0 mm diameter were fabricated in accordance with ASTM test procedure E 8 and pulled to failure at a strain rate of 0.5 mm min⁻¹. Tensile specimens smaller than 1.0 mm diameter (Ti-20Y only) could not be machined to comply with ASTM procedure E 8 and were tested with gauge length to diameter ratios larger than the ASTM standard 4:1 ratio. Such deviation from the standard procedure is believed to be conservative, yielding tensile strength measurements which may be lower than those from standard specimens. Specimens smaller than 1 mm diameter were tested at a strain rate of 0.25 mm min⁻¹.

Ductility values were determined by measuring tensile test fracture surface diameters with a traveling optical microscope and calculating the per cent reduction in area by comparison with the original diameter.

2.3. Specimen preparation for SEM and TEM stereology

Scanning electron microscopy (SEM) specimens were prepared by ordinary metallographic techniques and examined in an unetched condition. The large disparity in atomic number between titanium and yttrium provided strong contrast when using back-scattered electron imaging. A Cambridge S-200 microscope was used for all SEM photography.

Transmission electron microscopy (TEM) specimens were thinned by ion milling on a liquid-nitrogen chilled stage. A Philips CM30 S/TEM operated at 300 kV was used for all TEM photography.

Quantitative stereology [12] to measure mean-free distance between phases was performed on Ti-50Y SEM samples for the as-cast and as-extruded specimens. TEM samples were used for measurements at η values greater than 4.0 to avoid undercounting small phases that might lie beneath the resolving power of the SEM.

3. Results and discussion

3.1. The effect of deformation on microstructure

Ti-50Y and Ti-20Y both displayed progressively finer microstructures with increasing amounts of

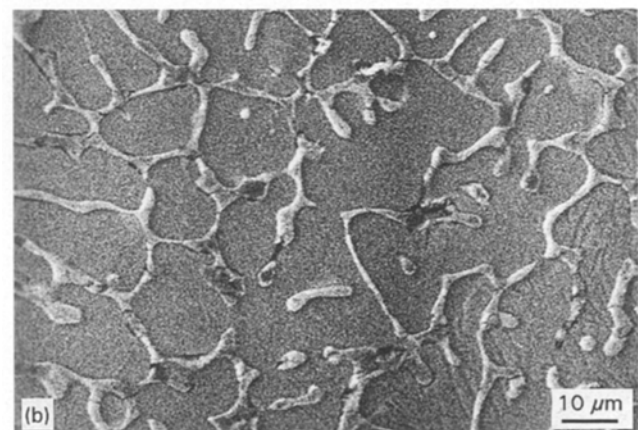
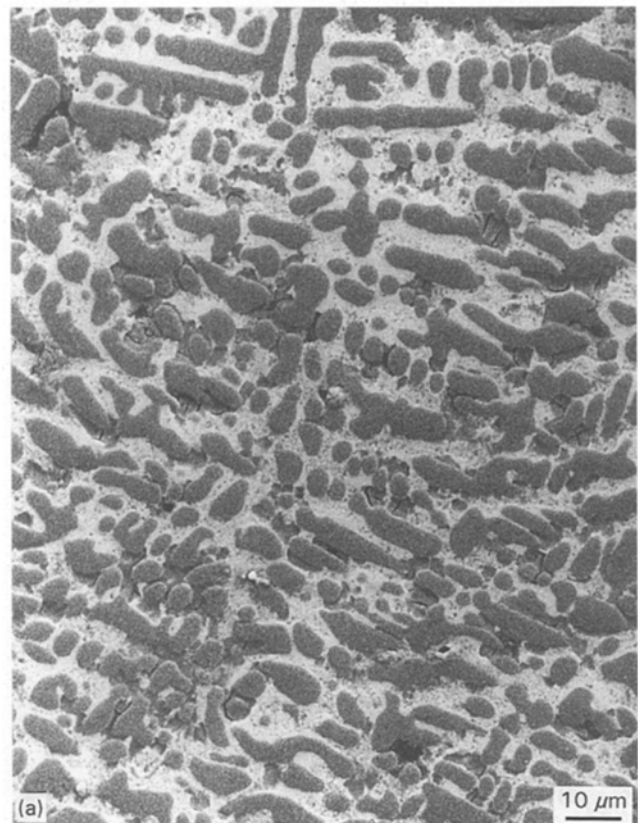


Figure 1(a) SEM back-scattered electron micrograph of as-cast Ti-50Y. The dark phase is titanium; the light phase is yttrium. Mean-free distance between phases in this specimen is 2.09 μ m. (b) SEM back-scattered electron micrograph of as-cast Ti-20Y.



Figure 2 SEM back-scattered electron micrograph of a transverse section of Ti-50Y extruded at 860 °C to $\eta = 2.8$. Mean-free distance between phases in this specimen is 890 nm.

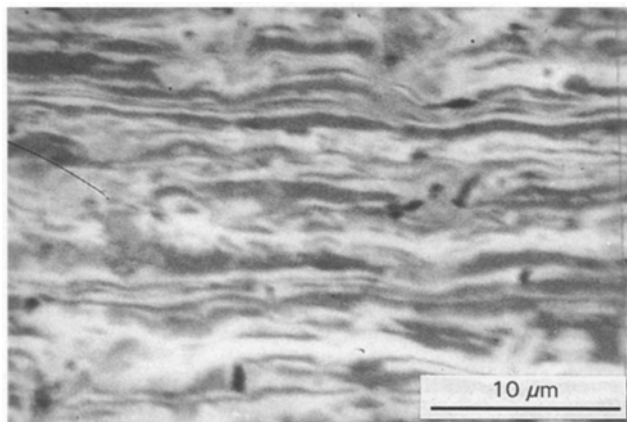


Figure 3 SEM back-scattered electron micrograph of a longitudinal section of Ti-50Y extruded at 860 °C to $\eta = 2.8$. Mean-free distance between phases in this specimen is 890 nm.

deformation. As cast, both alloys show a microstructure characteristic of two immiscible metals (Fig. 1a and b). Initial hot work changes the original dendritic structure to a filamentary structure similar to that observed in Cu-X *in situ* composites. This is illustrated in Figs 2 and 3, where the microstructure is shown after the initial extrusion to $\eta = 2.8$.

The size and spacing of the kinked filaments decreased with continuing deformation, resulting in the nanofilamentary microstructure seen in Figs 4–5. The Ti-50Y deformed by Path I (hot worked to $\eta = 4.8$ followed by cold work) showed no measureable difference from that deformed by Path II (hot worked to $\eta = 2.8$ followed by cold work) in either ultimate tensile strength or average phase spacing. At the high-



Figure 4(a, b) TEM bright-field micrographs of Path I Ti-50Y extruded at 860 °C to $\eta = 2.8$ and hot swaged at 725 °C to $\eta = 4.7$. Mean-free distance between phases in this specimen is 150 nm.

est levels of deformation achieved, the phases assume a more equiaxed structure (Figs 6 and 7), perhaps as a result of recrystallization during the many stress relief anneals performed on these specimens in the course of their cold swaging (Section 2.1).

X-ray texture analysis performed on the Ti-50Y alloy at $\eta = 2.8$ showed that both the titanium and

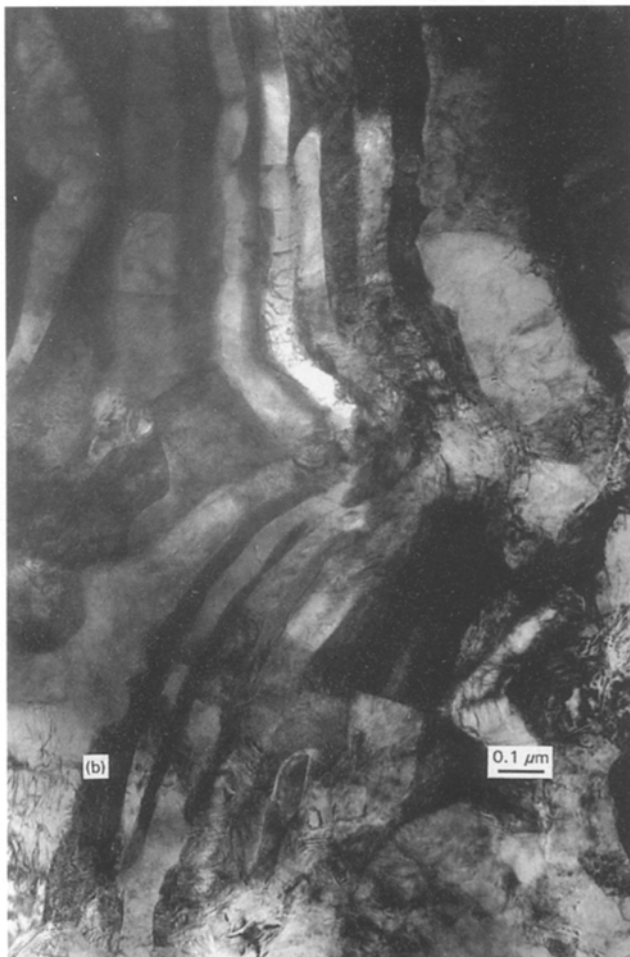
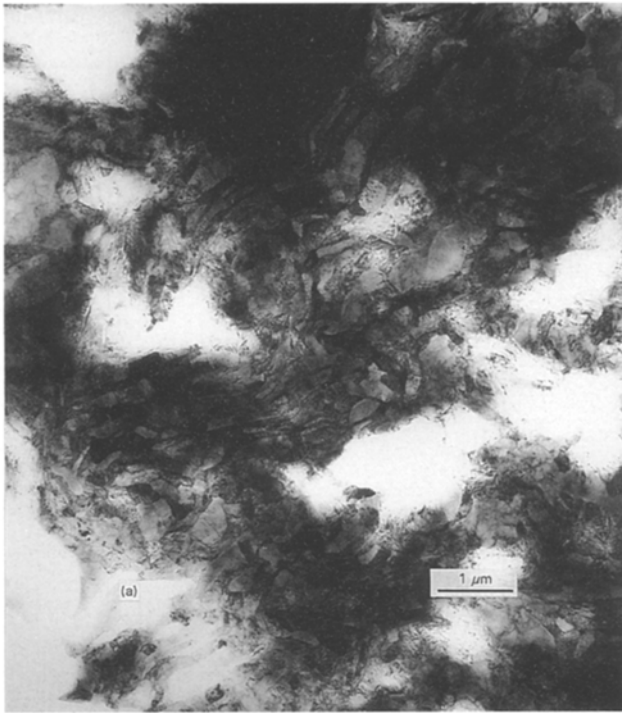


Figure 5(a, b) TEM bright-field micrograph of Path II Ti-50Y extruded at 860 °C to $\eta = 2.8$ and cold swaged (with periodic vacuum anneals at 615 °C) to $\eta = 4.6$. Mean-free distance between phases in this specimen is 145 nm.

ytrium phases were beginning to develop a $[10\bar{1}0]$ fibre axis texture. Unfortunately, the small size of the specimens prevents reliable texture analysis at higher η values.

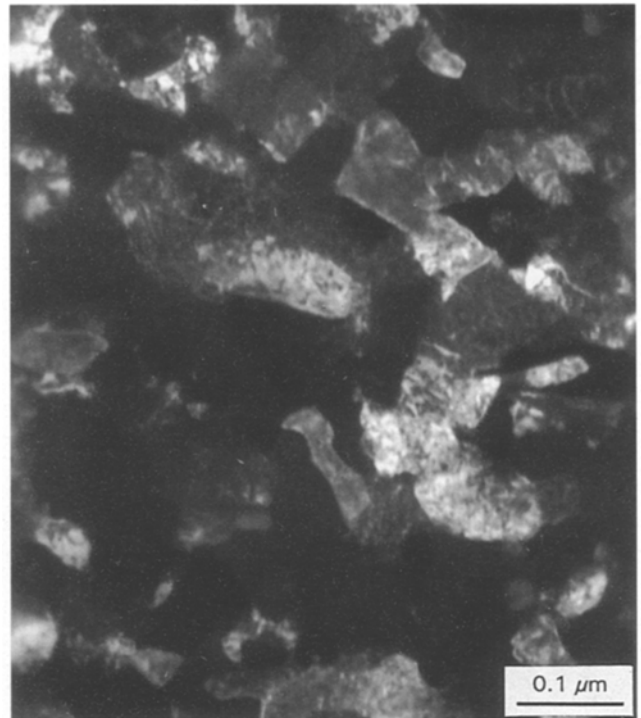


Figure 6 TEM conical scan dark-field micrograph of Ti-20Y ($\eta = 7.6$). Mean-free distance between phases in this specimen is 105 nm.



Figure 7 The same area shown in Fig. 8, in bright-field.

3.2. The effect of deformation on mechanical properties

Deformation processing substantially increased the ultimate tensile strength (UTS) of both alloys. Fig. 8 shows that each alloy approximately tripled in UTS, similar to the UTS increase seen in Cu-20Nb for similar η values. Ductility of the Ti-20Y alloy was superior to that of the Ti-50Y (Fig. 9), but the role of

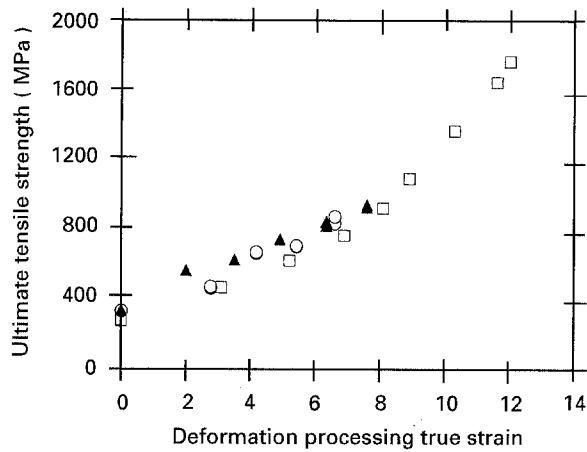


Figure 8 Comparison of the *in situ* strengthening effect for Path II (○) Ti-50Y, (▲) Ti-20Y, and (□) Cu-20Nb alloys.

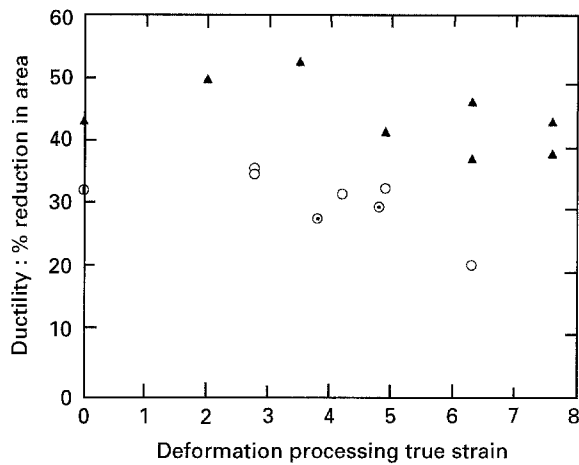


Figure 9 Ductility measured as per cent reduction in area for (▲) Ti-20Y and for Path (○) I and (○) II Ti-50Y as a function of η .

the yttrium content in determining ductility as well as UTS was unfortunately obscured by an inadvertent contamination of the Ti-50Y alloy with oxygen. Gas-fusion analyses of both alloys show that the Ti-20Y alloy interstitial content was low throughout the experiment, but the Ti-50Y ingot was apparently contaminated with oxygen during initial casting, and suffered further contamination during deformation processing and vacuum annealing (Table I).

Quantitative stereology on Paths I and II Ti-50Y alloy indicated that the UTS of Ti-50Y does not increase as rapidly with decreasing mean free distance between phases, as is the case in Cu-20Nb; but here again, because dissolved oxygen is a potent strengthening agent in titanium, the 900 p.p.m O increase in this alloy during deformation confuses the result. In an attempt to quantify the relation between filament spacing and UTS, the UTS of Path II Ti-50Y is plotted in Fig. 10 as a function of average phase spacing. In Cu-20Nb rods, the UTS was found to increase as a function of [6] $\lambda^{-0.37}$, where λ is the mean free distance between niobium phases, rather than the thickness of the niobium phases, but in a Ti-50Y composite, no such distinction is needed because the titanium and yttrium have

TABLE I Contamination during deformation processing and vacuum annealing

Alloy η	Oxygen (wt in p.p.m)	Nitrogen (wt in p.p.m)	Hydrogen (wt in p.p.m)
Ti-50Y			
0	2100	110	37
4.8	2100	110	48
6.6	3000	100	110
Ti-20Y			
0	480	46	77
7.6	560	280	41

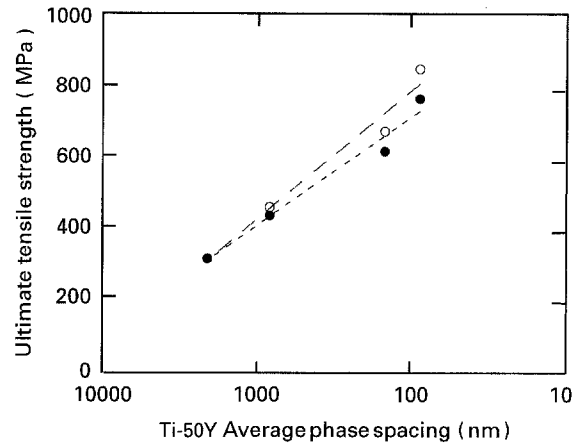


Figure 10 Ultimate tensile strength of Paths I and II Ti-50Y as a function of mean free distance between phases. (—○—) Measured values; (—●—) measured values after applying estimated correction factor for the strengthening effect of the increased oxygen content observed in this alloy (see Section 3.2).

nearly identical densities and are present in equal volumes and weights in the Ti-50Y alloy. UTS and filament spacing data for the Ti-50Y alloy (Path II) show a lower strengthening effect with the UTS measured increasing as a function of (mean free distance between phases)^{-0.29}. If one assumes that an increase in oxygen content from 2100 p.p.m. to 3000 p.p.m. would impart an 85 MPa strengthening effect in titanium [13] (and assuming a similar effect in yttrium), the "corrected" effect of mean-free distance between phases for Path II Ti-50Y can be estimated to increase as a function of (mean free distance between phases)^{-0.26}.

The quantitative stereology on the Ti-20Y (Fig. 11) showed an increase in UTS as a function of (mean free distance between phases)^{-0.22}. The value obtained for the Ti-20Y alloy may be more meaningful, because that specimen had essentially constant oxygen content throughout the deformation process.

The strengthening of Cu-Nb composite that occurs with decreasing distance between phases has been partially attributed to the pronounced texturing observed in the fcc copper matrix and the bcc niobium second phase [1]. The copper matrix forms a mixed texture with [001] and [111] fibre axes, while the niobium forms a preferred orientation along a [110] fibre axis. These textures, in turn, develop a helically twisted niobium filament because the copper deforms nearly axisymmetrically while the niobium is constrained to employ only the two <111> slip directions

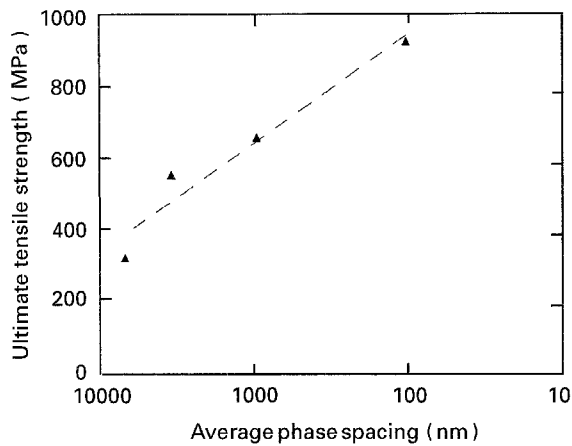


Figure 11 Ultimate tensile strength of Ti-20Y as a function of mean-free distance between phases.

that are not perpendicular to the axis of the rod. Simply put, the angle of alignment of the slip systems in textured copper and niobium is unfavourable for propagating dislocations across the phase boundary. This crystallographic arrangement makes the Cu-Nb phase boundaries into effective barriers to dislocations. For the given texture which develops in the copper matrix, Schmidt factor calculations show [14] that the majority of dislocation movement will be on slip planes that intersect the twisted morphology of the niobium filaments, rather than along the fibre axis where no barriers are present. Thus, dislocation movement is restricted to distances of the order of the filamentary spacing. If this spacing is too small, it may be impossible to generate dislocations [15].

The situation in Ti-Y composite must differ considerably from that of Cu-Nb. In Ti-Y composites, both constituents are hcp and have identical c/a ratios of 1.587. If the normally observed $[10\bar{1}0]$ fibre axis for hcp metals were to form in both the titanium and yttrium, the preferred slip system active for the room-temperature tensile testing performed in this study would be $\{10\bar{1}0\} \langle 11\bar{2}0 \rangle$. It is assumed that basal slip would not play a major role in deformation because a $[10\bar{1}0]$ fibre axis would orient the basal plane unfavourably for slip and the critical resolved shear stress for basal slip in titanium is substantially higher than for the $\{10\bar{1}0\} \langle 11\bar{2}0 \rangle$ system [16]. In contrast to the textured copper and niobium slip systems of the Cu-Nb composites, the textured titanium and yttrium slip systems would both be oriented at a 60° angle to the rod axis, but propagation of dislocations across a Ti-Y phase boundary would still be impeded by the 24% difference between the titanium and yttrium lattice parameters and random variations in alignment of the slip systems caused by their remaining degree of freedom to rotate about the rod axis. These factors might account for the somewhat lower rate of strengthening with decreasing phase spacing seen in the Ti-Y composites *vis-a-vis* the Cu-Nb composite.

An additional factor in the more rapid strengthening observed with deformation in Cu-Nb may be the convoluted shape of the niobium filaments. This spiralling, fluted interface between the copper and ni-

bium presumably impedes dislocations more effectively than the relatively smoother interface observed between titanium and yttrium. While it is difficult to quantify the degree of twisting observed in the filaments, the smoother, less-convoluted filaments in the Ti-Y composites may produce a larger effective spacing seen by dislocations. On a smaller scale the filaments are expected to approximate more closely a lamellar structure, where dislocation movement in all directions in the plane of the lamellae is unhindered [14]. The strengthening effect of the filaments is therefore expected to be somewhat lower, similar to what is seen in rolled Cu-Nb sheet, which has been shown to exhibit a lower strengthening effect with filament spacing [17].

Although no quantitative data were taken on dislocation densities in the Ti-Y composites, the dislocation density observed on the TEM foils appeared similar to the 10^{10} cm^{-2} seen in the Cu-Nb composites. Any large increases in dislocation density which may be occurring upon deformation are presumably eliminated from the structure by the frequent anneals to which the material was subjected.

4. Conclusion

This preliminary study has demonstrated that: (1) Ti-20Y and Ti-50Y can be cast and deformation processed to true strains of 7.6 and 6.6, respectively, to produce nanofilamentary microstructures; and (2) this deformation processing results in UTS increases similar to those seen in the well-studied Cu-20Nb alloy for equivalent true strains.

The Cu-X alloys exhibit their greatest strengthening effect at high deformation levels ($\eta = 10-13$) where phase spacings are in the range of a few tens of nanometres. It remains to be seen if these Ti-Y alloys will tolerate such high true strains and, if they do, whether very high tensile strengths will result. Experiments are currently underway to attempt deformation processing to higher η values on large-diameter (75 mm) cast ingots of low-oxygen Ti-Y alloys and a control sample of pure titanium. It is hoped that such data will help discriminate strengthening effects caused by work hardening in single-phase material from the effect of the nanofilamentary microstructures of the two-phase alloys. In addition, these larger samples should provide X-ray texture analysis data that may clarify the effect of preferred orientation on the mechanical behaviour of these alloys.

Acknowledgements

The authors thank J. D. Verhoeven, F. A. Schmidt, L. L. Jones, L. P. Lincoln, L. K. Reed and J. T. Wheelock, of Ames Laboratory, for their valuable discussions and for preparing the materials used in this study. This work was performed at Ames laboratory, operated for the US Department of Energy by Iowa State University under contract W-7405-ENG-82 with additional financial support from the Engineering Research Institute of Iowa State University.

References

1. J. BEVK, J. P. HARBISON and J. L. BELL, *J. Appl. Phys.* **49** (1978) 6031.
2. J. D. VERHOEVEN, F. A. SCHMIDT, E. D. GIBSON and W. A. SPITZIG, *J. Metals* **38** (1986) 20.
3. J. D. VERHOEVEN, W. A. SPITZIG, L. L. JONES, H. L. DOWNING, C. L. TRYBUS, E. D. GIBSON, L. S. CHUMBLEY, L. G. FRITZMEIER and G. D. SCHNITTGRUND, *J. Mater. Eng.* **12** (1990) 127.
4. W. A. SPITZIG and P. D. KROTZ, *Acta Metall.* **36** (1988) 1709.
5. J. D. VERHOEVEN, W. A. SPITZIG, F. A. SCHMIDT and C. L. TRYBUS, *Mater. Manuf. Process.* **4** (1989) 197.
6. J. D. VERHOEVEN, W. A. SPITZIG, F. A. SCHMIDT, P. D. KROTZ and E. D. GIBSON, *J. Mater. Sci.* **24** (1989) 1015.
7. P. D. FUNKENBUSCH and T. H. COURTNEY, *Acta Metall.* **33** (1985) 913.
8. L. S. CHUMBLEY, H. L. DOWNING, W. A. SPITZIG and J. D. VERHOEVEN, *Mater. Sci. Eng.* **A117** (1989) 59.
9. C. L. TRYBUS, L. S. CHUMBLEY, W. A. SPITZIG and J. D. VERHOEVEN, *Ultramicroscopy* **30** (1989) 315.
10. P. D. FUNKENBUSCH and T. H. COURTNEY, *Scripta Metall.* **23** (1989) 1719.
11. W. A. SPITZIG, J. D. VERHOEVEN, C. L. TRYBUS and L. S. CHUMBLEY, *Scripta Metall. Mater.* **24** (1990) 1171.
12. E. E. UNDERWOOD, "Quantitative Stereology" (Addison-Wesley, Reading, Mass., 1970) Chs 3 and 4.
13. M. J. DONACHIE Jr, "Titanium: A Technical Guide" (ASM International, Metals Park, OH, 1988) pp. 40–1.
14. L. S. CHUMBLEY, unpublished work (1990).
15. J. S. KOEHLER, *Phys. Rev.* **B2** (1970) 547.
16. E. A. ANDERSON, D. C. JILLSON and S. R. DUNBAR, *Trans. AIME* **197** (1953) 1191.
17. C. L. TRYBUS, PhD dissertation, Iowa State University (1988) 75.

*Received 9 September 1993
and accepted 5 September 1994*